ROYAL SOCIETY
OF CHEMISTRY

PAPER

Check for updates

BiOBr hybrids for organic pollutant removal by the combined treatments of adsorption and photocatalysis

Yichang Yu,[a] Chengjun Li,[a] Shoushuang Huang,[b] Zhangjun Hu,*[ab] Zhiwen Chen [ID][b] and Hongwen Gao [ID] *[a]

The xSiO$_2$–BiOBr ($x = 0$–5) and SN–SiO$_2$–BiOBr hybrids were synthesized *via* a facile one step co-precipitation method. To determine the optimal formula, the photocatalytic degradation of C. I. reactive red 2 (X3B) with xSiO$_2$–BiOBr ($x = 0$–5) was investigated. Under simulated sunlight irradiation, 4SiO$_2$–BiOBr exhibited a better photocatalytic efficiency than other materials; 1.77 and 1.51 times higher than conventional nano TiO$_2$ and pure BiOBr, respectively. To demonstrate the photocatalytic degradation mechanism, the effect of active species on degradation of X3B was carried out, and a possible degradation pathway was proposed. To realize the combined treatments of adsorption and photocatalysis, an inorganic/organic (I/O) SN–SiO$_2$–BiOBr hybrid was further strategized and synthesized. It showed much better adsorption performance than the SiO$_2$–BiOBr composite. It could enrich organic pollutants by facile adsorption, and then degrade them to H$_2$O and CO$_2$ under natural sunlight irradiation. Notably, this sunlight-driven photocatalysis can be performed in the slurry resulted from the pollutant adsorption. As a result, the proposed combination of adsorption and photocatalysis will provide a novel strategy to greatly facilitate the treatment of organic wastewater.

1. Introduction

The rapid development of society has been causing severe environmental problems. More and more pollutants are being created by human activity. The produced pollutants are damaging the quality of air, water, soil and so on.[1] In particular, organic pollutants are of global concern due to their potential for long-range transport, persistence and ability to bio-magnify and bio-accumulate in ecosystems, as well as their significant negative effects on human health.[2] It is well known that the semiconductor photocatalysis technique is an effective and environment-friendly method to eliminate organic pollutants.[3–7] Recently, photocatalysis has received widespread attention.

Bismuth-based photocatalysts, one type of semiconducting material, have been extensively investigated in different contexts by many researchers.[8–11] In order to improve their photocatalytic efficiency, many efforts for the optimization have been made, such as morphology modification, doping, combination and so on.[12–15] For instance, Haider *et al.*[16] reported that unique octagonal shaped BiOCl nanosheets dominantly exposing with (001) facets exhibited 2.8 times higher

photocatalytic efficiency than that of pristine BiOCl. Huo *et al.*[17] prepared hierarchical flower-like BiOBr microspheres, which exhibited an excellent durability and high photocatalytic activity. The visible-light absorbance was significantly enhanced due to the light multi-reflections, high separation efficiency of photo-generated electrons and holes, high crystallization and the large surface area. Gnayem and Sasson[18] fabricated BiOCl$_x$Br$_{1-x}$ by a co-precipitate method at room temperature. They found that fabrication protocol and raw materials strongly effected the structure and performance of BiOCl$_x$Br$_{1-x}$. The alloy BiOCl$_{0.875}$Br$_{0.125}$ showed a highly visible photocatalytic activity toward rhodamine B. Mi *et al.*[7] synthesized Fe(III) modified BiOCl ultrathin nanosheets *via* a facile solvothermal approach. The nanosheet was less than 5 atomic layer with the exposure of active facets (001), which further enhanced the separation and transfer efficiency of charge carriers. Therefore, it presented an excellent performance for both photocatalytic degradation and water splitting. In recent years, BiOBr has attracted increasing attention in the photocatalysis field owing to its wide adsorbing wavelength.[19–25] Di *et al.*[26] prepared a novel nitrogen-doped carbon quantum dots/BiOBr ultrathin nanosheets by an ionic liquid assisted solvothermal process. The enhanced photocatalytic performance was attributed to the increased light harvesting capacity, excellent electron transfer ability. Li *et al.*[27] synthesized hollow mesoporous SiO$_2$–BiOBr *via* a facile three-step method, the results indicated that the photocatalytic activity of this hollow mesoporous SiO$_2$–BiOBr was more superior than that of the core–shell SiO$_2$@mSiO$_2$-BiOBr

[a]State Key Laboratory of Pollution Control and Resource Reuse, College of Environmental Science and Engineering, Tongji University, Shanghai 200092, PR China. E-mail: hwgao@tongji.edu.cn

[b]School of Environmental and Chemical Engineering, Shanghai University, Shanghai, 200444, PR China. E-mail: huzjun@shu.edu.cn

This journal is © The Royal Society of Chemistry 2018

under visible-light irradiation. Zhang et al.[28] investigated the photocatalytic degradation efficiency of BiOBr@SiO$_2$@Fe$_3$O$_4$ for 2,2-bis(4-hydroxyphenyl)propane (BPA), which was superior to that of commercial TiO$_2$ (P25). And a detailed degradation pathway of BPA degradation was proposed. Besides, Yao[29] and Li[30] prepared BiOBr@SiO$_2$@Fe$_3$O$_4$ via different multi-step processes, these materials all had very good photocatalytic performance. Modifying BiOBr with silicon dioxide is a promising way to improve the photocatalytic performance. However, all these silicon dioxide combined photocatalysts were prepared by hydrothermal method, which was energy-hogging. Besides, the whole reactions were complicated, which had three steps.

Although photocatalysis technique has its own advantages and many works have been done for the photocatalytic efficiency promotion, there are still many issues for the practical application in wastewater treatments. If the organic pollutants from wastewater can be enriched by photocatalysts, then the enriched pollutants are separated and further degraded by photocatalytic technology, it would dramatically reduce the processing capacity and greatly facilitate the treatment. Therefore, the multifunctional materials with both good adsorption and photocatalytic capabilities are demanded. However, pure inorganic photocatalysts commonly have limited adsorption capacities.[31–33] Inorganic–organic (IO) composite materials, combining the characteristics of both inorganic and organic substances, show numbers of advantages in adsorption capacity.[34] Our group synthesized the octadecyl dimethyl hydroxyethyl quaternary ammonium (SN) hybridized silicate, and it exhibited a high adsorption capacity towards anionic and amphoteric dyes. In addition, the dye sludge can be used for antistatic colorant.[35] Besides, SN@SiO$_2$ was developed for adsorption of sulfuric dye and nonylphenol. This composite had high adsorption capacity and fast adsorption rate.[36]

Based on the aforementioned consideration, a facile one step co-precipitation method was proposed to prepare lamella accumulational SiO$_2$–BiOBr composite. It exhibited a highly superior photoactivity for the degradation of X3B in an aqueous system. Moreover, the effect of sodium metasilicate and main active species were investigated. The I/O SN–SiO$_2$–BiOBr with both good adsorption and photocatalytic performance was further designed and synthesized. Firstly, this I/O composite was used to control dyes wastewater by adsorption, then the supernatant was removed and the concentrated slurry was exposed to natural sunlight for the degradation of dyes. The photocatalytic process for the degradation of dyes wastewater was changed from aqueous system to solid system for the first time. It provided a novel and green way to treat with organic pollutants in environmental water.

2. Experimental

2.1 Materials and reagents

Bismuth nitrate pentahydrate, ethylene glycol (EG), sodium metasilicate (Aladdin Agents, China) and absolute ethanol (EtOH), potassium bromide (Sinopharm Chemical Reagent), SN (Zhejiang Runtu Co., China) were used for the preparation of SiO$_2$–BiOBr and SN–SiO$_2$–BiOBr. X3B (Shanghai GreenEmpire

EP S&T Co., China) were used for the adsorption and photodegradation test. Isopropyl alcohol (IPA), tert-butanol (TBA), 1,4-benzoquinone (BQ) and potassium iodide (Aladdin Agents, China) were used for the investigation of photocatalysis mechanism. All these reagents were used without further treatment.

2.2 Preparation of SiO$_2$–BiOBr

The composite was prepared by a simple co-precipitation method with Bi(NO$_3$)$_3$·5H$_2$O, KBr and Na$_2$SiO$_3$·9H$_2$O as Bi, Br and Si source, respectively. Briefly, 4 mM KBr and a certain amount of Na$_2$SiO$_3$·9H$_2$O were dissolved in 50 mL deionized water. 4 mM Bi(NO$_3$)$_3$·5H$_2$O was dissolved in a mixed solution of EG (15 mL) and EtOH (15 mL) under stirring at room temperature. After Bi(NO$_3$)$_3$·5H$_2$O was completely dissolved, it was added to the mix solution. The reaction was allowed to proceed at room temperature for 1 h under continuous stirring. After stationarity aging for 12 h at room temperature, the resulting precipitate was washed with deionized water and EtOH for several times, and dispersed in 20 mL deionized water. The amount of Na$_2$SiO$_3$·9H$_2$O was 0, 1, 2, 3, 4, 5 mM, respectively. Herein, the products were denoted as xSiO$_2$–BiOBr (x = 0, 1, 2, 3, 4, 5).

2.3 Preparation of SN–SiO$_2$–BiOBr

4 mM KBr, 4 mM Na$_2$SiO$_3$·9H$_2$O and a certain amount of SN were dissolved in 50 mL deionized water. 4 mM Bi(NO$_3$)$_3$·5H$_2$O was dissolved in a mixed solution of EG (15 mL) and EtOH (15 mL) under stirring at room temperature. After Bi(NO$_3$)$_3$·5H$_2$O was completely dissolved, it was added to the mix solution. The reaction was allowed to proceed at room temperature for 1 h under continuous mechanical stirring. After stationarily aging for 12 h at room temperature, the resulted precipitate was washed with deionized water and EtOH for several times, and dispersed in 20 mL deionized water.

2.4 Characterization

The samples were characterized by X-ray powder diffraction (XRD) on a powder diffractometer (Equinoxss/hyperion 2000, Bruker Co., Germany). Scanning electronic microscopy (SEM) (Model Quanta 200 FEG, FEI Co. USA) was used to measure the size and shape of the hybrid sorbents. Transmission electron microscopy (TEM) (Model TECNAI G2, S-TWIN, FEI Co. USA) was used to characterize the morphology of samples. The infrared spectroscopy (IR) spectra were measured with a Fourier transform infrared spectrometer (Model NICOLET 5700, Thermo Electron Co. USA) to demonstrate that SN was embedded into the hybrid materials. The elemental analysis device (Model Vario EL III, Germany) was used to determine C, N and H content. A photodiode array spectrometer (Model S4100, Scinco, Korea) with the Labpro plus software (Firmware Version 060105) was used to determine the concentration of X3B solutions.

2.5 Performance test

The photocatalytic degradation experiments were carried out in a photochemical reactor. In a typical experiment, 25 mg sample was dispersed in 50 mL dye (20 mg L^{-1}) solution. A 500 W Xe

lamp was employed as light source. Before photocatalytic activity test, the mix solution was placed in dark and stirred for 30 min to reach an adsorption–desorption equilibrium. Subsequently, at given time intervals, 5 mL solution was collected from the suspension and centrifuged. The concentration of X3B during the photocatalytic reaction was determined at 545 nm by spectrophotometer.

TBA was chosen as photoexcited e^- scavenger, BQ was chosen as $O_2^{\bullet-}$ scavenger, IPA was chosen as ·OH scavenger, and KI was chosen as h^+ scavenger. Typically, 25 mg of the catalyst was dispersed in X3B aqueous solution (50 mL, 20 mg L^{-1}) with 1 mM L^{-1} TBA, IPA, BQ and KI respectively. The reaction and measurement process was the same as above.

In adsorption experiment, 5 mg SN–SiO_2–BiOBr was added to 10 mL X3B solution. The concentration of X3B solution was 100, 130, 160, 200 and 250 mg L^{-1}, respectively. These mixtures were stirred for 30 min in the dark, then centrifuged and detected. For the test of slurry photocatalytic activity, the process was as follow: 0.1 g SN–SiO_2–BiOBr was added to 1000 mL 40 mg L^{-1} dye solution. The mix solution was placed in dark and stirred for 30 min. After stationarily standing for 1 h in the dark, the mix solution was concentrated to 40 mL slurry. The slurry was separated to eight equal parts. Each part 5 mL of the slurry was equably added to culture dish (75 mm). They were exposed under nature sunlight, some of them were dried at 90 °C for 2 h. Then the dried powder was collected. The C, N and H content of these dried powder were determined by elemental analysis.

3. Results and discussion

3.1 Characterization of photocatalyst

SEM images of as-synthesized samples are shown in Fig. 1. BiOBr is composed of many aggregated nanoplates. After combined with silicon dioxide, the morphology does not change much except 5SiO_2–BiOBr. The diameter of the $x$$SiO_2$–BiOBr ($x$ = 0, 1, 2, 3, 4) nanoplates decrease from 600 to 200 nm. 5SiO_2–BiOBr shows totally different morphology with other samples, which is composed of many disordered nanoparticles. The changes were contributed to the different basicity caused by the addition of sodium metasilicate. TEM images of as-synthesized samples are shown in Fig. 2. The $x$$SiO_2$–BiOBr ($x$ = 0, 1, 2, 3, 4) are composed with many nanoplates aggregated together, and the diameter of nanoplates decrease with the increase of silicon. These images were consistent with the SEM images. The clear lattice fringes is about 0.35 nm in the HRTEM images of 4SiO_2–BiOBr, which were in accordance with (101) planes of the tetragonal system of BiOBr.

Fig. 3 displays the powder XRD patterns of as-synthesized samples. The main diffraction peaks at about 10.8, 21.8, 25.2, 31.7, 32.2, 39.3, 46.3, 50.7, 53.4, 57.2 and 76.8° can be indexed to the (001), (002), (101), (102), (110), (112), (200), (104), (211), (212) and (310) planes of the tetragonal BiOBr (JCPDS Card No. 78-0348). The intense and sharp diffraction peaks suggest that the as-synthesized BiOBr in these samples are very well-crystallized. There are no other obvious peaks for SiO_2 which is attributed to the amorphous structure of SiO_2 plates.[29] In order to further investigate the composition of as-synthesized samples, the XPS test has been taken. 4SiO_2–BiOBr was chosen as a representative, and BiOBr was chosen as blank control. As shown in Fig. 4A, there is only one peak at 530.9 eV, which is fitted with the characteristic peak of O_{1s} in BiOBr. And there are two peaks in Fig. 4C, except the one at 530.9 eV, the other one at 533.6 eV should be assigned to the characteristic peak of O_{1s} in SiO_2. This reveals the existence of SiO_2 in 4SiO_2–BiOBr. Furthermore, there is no peak for the element of Si in Fig. 4B, and there is an obvious peak for the element of Si in Fig. 4D. This results indicate SiO_2 is successfully prepared in the composite. The atomic concentration of this two composites are shown in Table 1. The atomic concentration of BiOBr are 34.06, 0.00, 25.63 and
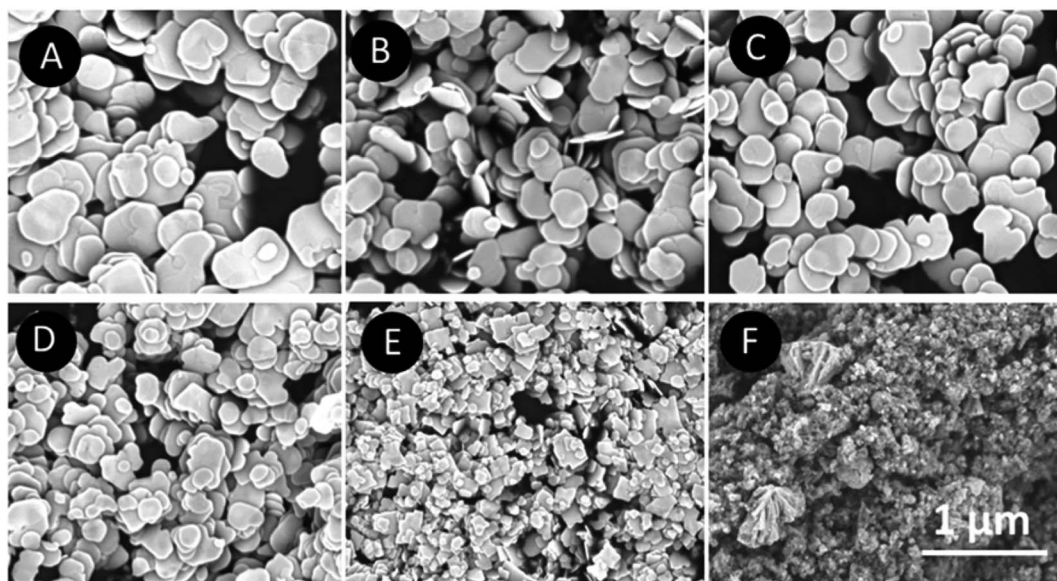

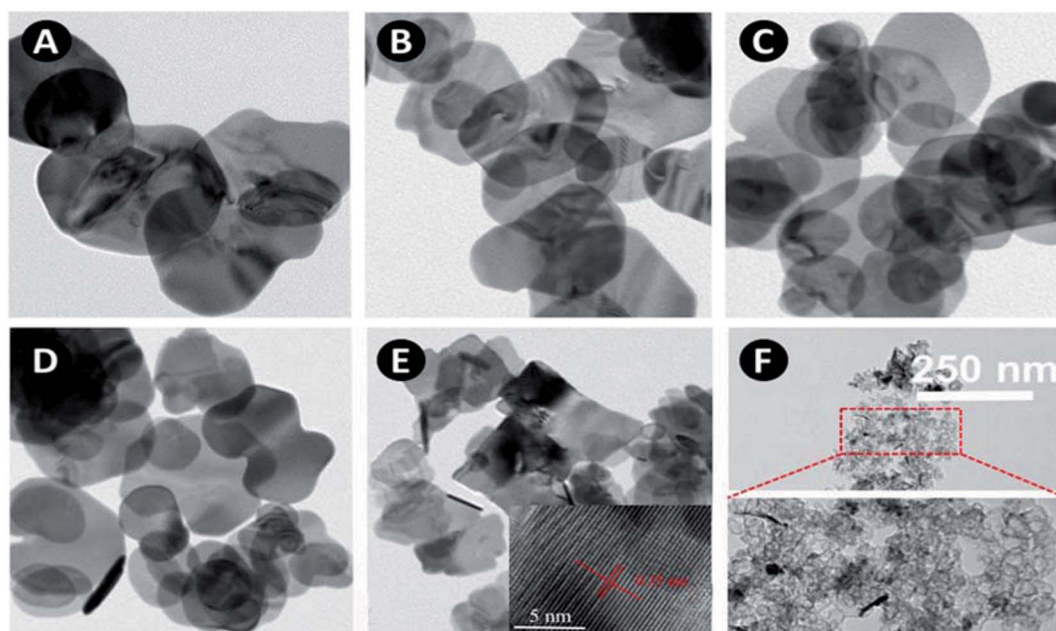Fig. 1 SEM images of $x$$SiO_2$–BiOBr ($x$ = 0, 1, 2, 3, 4, 5) (A–F).

Fig. 2 TEM images of xSiO$_2$–BiOBr (x = 0, 1, 2, 3, 4, 5) (A–F) and HRTEM image inset of panel (E).

40.31 for O, Si, Br and Bi, respectively, which are 52.28, 13.41, 14.02 and 20.29 for 4SiO$_2$–BiOBr. These results demonstrate the existence of SiO$_2$ and reveal their composition.

3.2 Photocatalytic performance

X3B was chosen as a representative target organic pollutant to evaluate the photocatalytic performance of as-synthesized samples. Fig. 5A displays the corresponding photocatalytic degradation curves. The photocatalytic efficiency of samples increases with the increase of sodium metasilicate adding amount from 0 to 4 mM. 4SiO$_2$–BiOBr shows the best photocatalytic performance. The photocatalytic efficiency extremely reduces from 92% to 58.9% when the adding amount of sodium metasilicate is up to 5 mM. The addition of sodium metasilicate

can affect the final pH value and the amount of SiO$_2$. So the effect of pH value and amount of SiO$_2$ on the performance of samples need to be investigated. The pH value was 12.66 when 4 mM Na$_2$SiO$_3$·9H$_2$O was dissolved in 50 mL deionized water. The other two samples were prepared for comparison. One was denoted as 4SiO$_2$–BiOBr-7. The synthetic method was almost the same with that of 4SiO$_2$–BiOBr, except the mix solution of Na$_2$SiO$_3$·9H$_2$O and KBr was finally adjusted to pH 7 with 2 M HCl. And the other one was denoted as BiOBr-12.66, without the addition of Na$_2$SiO$_3$·9H$_2$O and the solution of KBr was adjusted to pH 12.66 with 2 M NaOH. These two samples were compared with 4SiO$_2$–BiOBr and pure BiOBr in photocatalytic performance for X3B. As shown in Fig. 5B, 4SiO$_2$–BiOBr has better photocatalytic performance than others. Compared with 4SiO$_2$–BiOBr-7, the only difference is pH value, which means that pH value can affect the photocatalytic performance of material. And when the pH value are same, for example 4SiO$_2$–BiOBr-7 and BiOBr, BiOBr-12.66 and 4SiO$_2$–BiOBr, the samples with SiO$_2$ have better photocatalytic performance. These indicate that the existence of SiO$_2$ improves the photocatalytic performance of BiOBr.

As shown in Fig. 6A, in dark condition the removal rates of X3B are about 45% and 20% respectively for nano TiO$_2$ and 4SiO$_2$–BiOBr. Nano TiO$_2$ has better adsorption performance for its nano structure. However, 4SiO$_2$–BiOBr shows much better photocatalytic performance than that of nano TiO$_2$. Under 70 min simulator solar irradiation, the removal rate of X3B for 4SiO$_2$–BiOBr is 95%, which is just 55% for nano TiO$_2$. And X3B can hardly be degraded by simulated sunlight without the addition of photocatalyst.

To investigate the effect of main active species during the photocatalytic process, a series of photodegradation experiments with the addition of different scavengers were carried
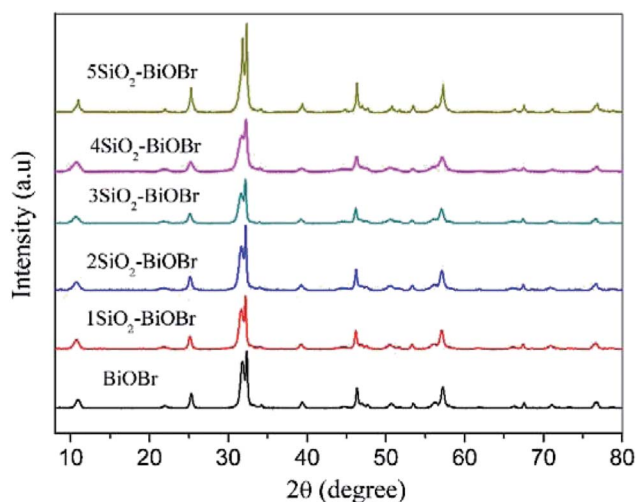

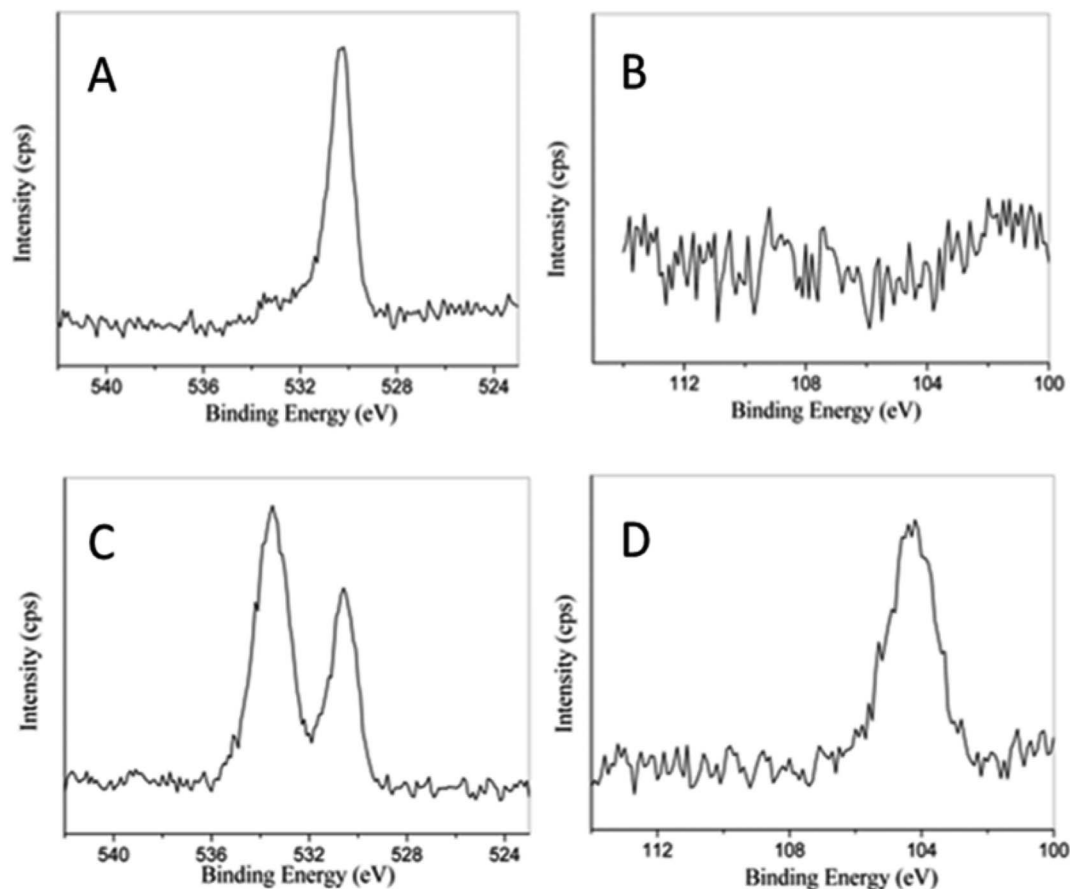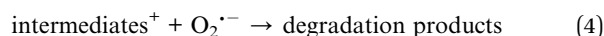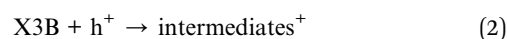**Fig. 3** XRD patterns of as-synthesized samples.

Fig. 4 XPS spectra of BiOBr (A and B) and $4SiO_2$–BiOBr (C and D) for the elements of O and Si, repectively.

out. As shown in Fig. 6B, when TBA or IPA was added into the degradation system, the photodegradation activity only had a slight decrease. It demonstrates that the e^- and ·OH are not the main active species. When KI was added into the degradation system, an obvious decrease in photoactivity was observed, and the corresponding removal rate decreased significantly from 95.9% to 62.4% in 40 min irradiation. This indicates that h^+ plays an important role in the degradation process. Besides, the adsorption efficiency of X3B decreased from 28.1% to 10%. When BQ was added into the degradation system, there was no obvious difference during the dark reaction, but the photocatalytic activity was totally different, the absorption at 545 nm increased with the increase of the reaction time. This indicates that the $O_2^{·-}$ radicals are the main active for X3B photodegradation on $4SiO_2$–BiOBr. Without the $O_2^{·-}$ radicals, the X3B could transfer to other forms of derivatives, which will result in the adsorption increased in the range of 520–560 nm. Therefore, in this photocatalytic degradation system, the possible photocatalytic mechanisms are proposed as follow:

Table 1 Atomic concentration of $4SiO_2$–BiOBr and BiOBr by XPS

Element	O	Si	Br	Bi
BiOBr	34.06	0.00	25.63	40.31
$4SiO_2$–BiOBr	52.28	13.41	14.02	20.29

$$\text{photocatalyst} + h\nu \rightarrow \text{photocatalyst (h}^+ + \text{e}^-) \quad (1)$$

$$\text{X3B} + \text{h}^+ \rightarrow \text{intermediates}^+ \quad (2)$$

$$\text{O}_2 + \text{e}^- \rightarrow \text{O}_2^{·-} \quad (3)$$

$$\text{intermediates}^+ + \text{O}_2^{·-} \rightarrow \text{degradation products} \quad (4)$$

Under simulated sunlight irradiation, the reaction is initiated with the excitation of $4SiO_2$–BiOBr photocatalyst, resulting in the promotion of electrons from the valence band (VB) to the conduction band (CB) of the BiOBr semiconductor and the generation of h^+ in the VB (eqn (1)). The h^+ reacts with X3B molecules to form intermediates$^+$ (eqn (2)). Oxygen molecules capture electrons to form $O_2^{·-}$ radicals (eqn (3)). Then the intermediates$^+$ react with $O_2^{·-}$ radicals to form the ultimate products, such as CO_2 and H_2O.

3.3 Characterization of SN–SiO₂–BiOBr

As we investigated above, $4SiO_2$–BiOBr composite is very promising on the photodegradation of organic pollutants. However, in the practical applications, there is still a challenge for the treatment of huge capacity of wastewater. The combining use of adsorption and photocatalysis will be a potential approach to solve this issue. Therefore, the IO SN–SiO₂–BiOBr hybrid was further constructed, which had both
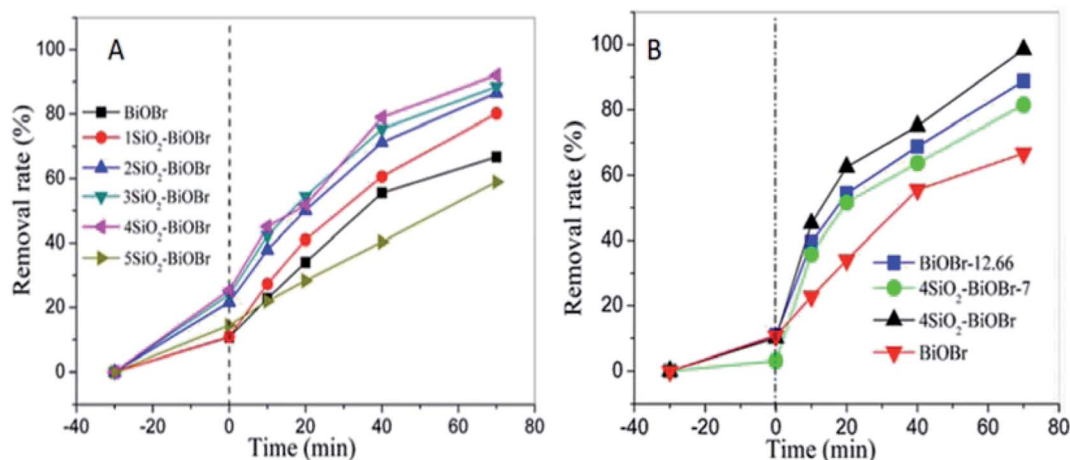
Fig. 5 Photocatalytic degradation of X3B in comparison to control experiments (A). Effects of SiO_2 and pH on the photocatalytic activity for X3B (B).

absorption and photocatalysis capabilities; and the effect of SN addition on the morphology and performance of $4SiO_2$–BiOBr were investigated. Fig. 7A shows the SEM images of SN–SiO_2–BiOBr, which is totally different with $4SiO_2$–BiOBr. It looks like a honeycomb, composed by many nanoparticles. There are many obvious pores on its surface. As shown in Fig. 7B, these nanoparticles piled up very thickly, which may make the BET surface area decrease. This change is contributed to the electric charge effect caused by SN.

The element analysis results of $4SiO_2$–BiOBr and SN–SiO_2–BiOBr are shown in Table 2. The content of C, N and H for $4SiO_2$–BiOBr is 0.759, 0.045 and 0.083%, respectively. The content of C, N and H for SN–SiO_2–BiOBr is 13.98, 1.352 and 2.896%, respectively. These results indicate SN is successfully combined with $4SiO_2$–BiOBr, and the content of SN is about 18%.

Fig. 8A and B display the N_2 adsorption/desorption isotherms of $4SiO_2$–BiOBr and SN–SiO_2–BiOBr. They both accord with the classical type IV isotherm, which refers to the most widespread adsorption behavior of the mesoporous

materials. The BET surface area for SN–SiO_2–BiOBr is 38.73 m^2 g^{-1}, and 83.53 m^2 g^{-1} for $4SiO_2$–BiOBr. The obvious decrease in the BET surface after the modification of SN can be observed, which should be caused by the morphology change. As shown in Fig. 8a and b, the BJH pore diameter of $4SiO_2$–BiOBr and SN–SiO_2–BiOBr nanophotocatalyst are determined to be 13.98 and 23.1 nm, respectively. Obviously, the significant increase of the pore size is also a key factor for the decrease of the BET surface area. The addition of SN and increased pore size of SN–SiO_2–BiOBr nanophotocatalyst can improve the adsorption ability to some extent. The XRD patterns of $4SiO_2$–BiOBr and SN–SiO_2–BiOBr are displayed in Fig. 8C. They have same peaks at 10.8, 25.2, 31.7, 32.2, 46.3, 50.7, 57.2 and 76.8°, which can be attributed to the reflection of the (001), (101), (102), (110), (200), (104), (212) and (310) planes, respectively. These peaks are identical to the structure of the tetragonal BiOBr (JCPDS Card No. 78-0348). There are no other obvious peaks for SiO_2 which is attributed to the amorphous structure of the SiO_2 plates in SN–SiO_2–BiOBr.
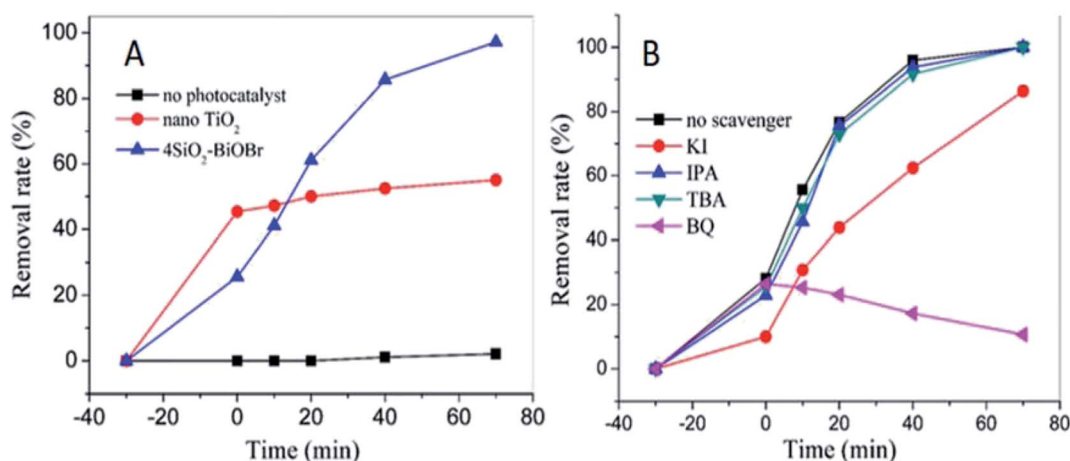

Fig. 6 The comparison of photocatalytic performance (A) effects of different scavengers on degradation of X3B in the presence of $4SiO_2$–BiOBr nanophotocatalyst under simulated sunlight irradiation (B).
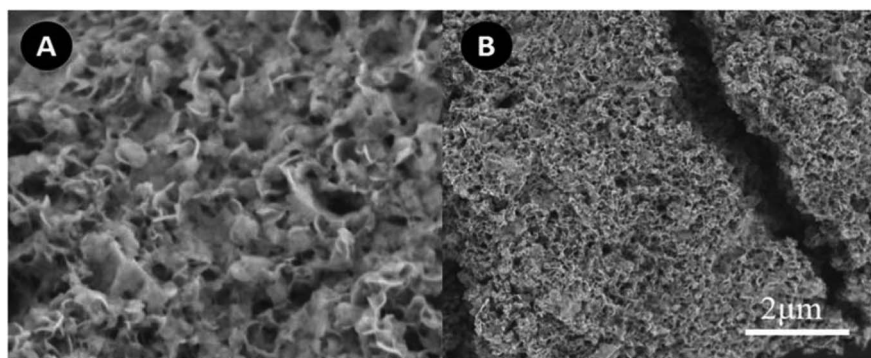
Fig. 7 SEM images of SN–SiO$_2$–BiOBr (A and B).

Table 2 C, N and H contents of 4SiO$_2$–BiOBr and SN–SiO$_2$–BiOBr

Element	C/%	N/%	H/%
4SiO$_2$–BiOBr	0.759	0.045	0.083
SN–SiO$_2$–BiOBr	13.98	1.325	2.896

3.4   Adsorption and photocatalytic performance of SN–SiO$_2$–BiOBr

Fig. 9A displays the adsorption performance of SN–SiO$_2$–BiOBr for X3B under dark conditions. The insert image shows the removal rate gradually decreased with the increase of initial concentration. For 100 mg L^{-1} X3B the removal rate by SN–SiO$_2$–BiOBr is over 95%, which is much higher than the 20% removal rate by 4SiO$_2$–BiOBr for 20 mg L^{-1} X3B. The results are consistent with Freundlich isotherm model (Fig. 9B) $\ln q_e = k + \frac{1}{n}\ln c_e$, where c_e is the equilibrium molarity in mg L^{-1}, q_e is the saturation adsorbance of X3B in mg g^{-1}, k and n is the constant. The value of k and n are 5.11 and 11.44. After the adsorption equilibrium, 1000 mL 40 mg L^{-1} dye solution with 0.1 g sample was concentrated to 40 mL slurry. Then 5 mL slurry was exposed under nature sunlight for different time. Fig. 9C shows the corresponding photocatalytic degradation performance. After 1 h exposure the slurry was totally dry, this was the first time the photocatalytic reaction was
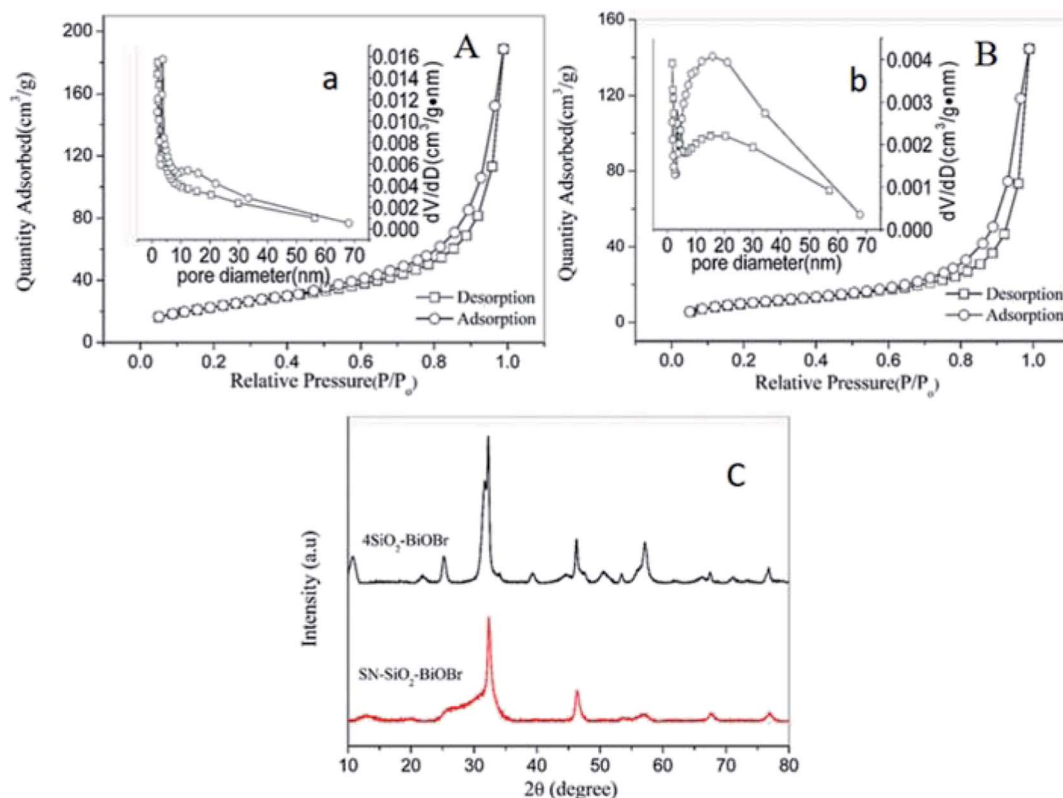

Fig. 8   N$_2$ adsorption/desorption isotherms and diameter distribution (b) of 4SiO$_2$–BiOBr (A and a) and SN–SiO$_2$–BiOBr (B and b), XRD spectra of 4SiO$_2$–BiOBr and SN–SiO$_2$–BiOBr (C).
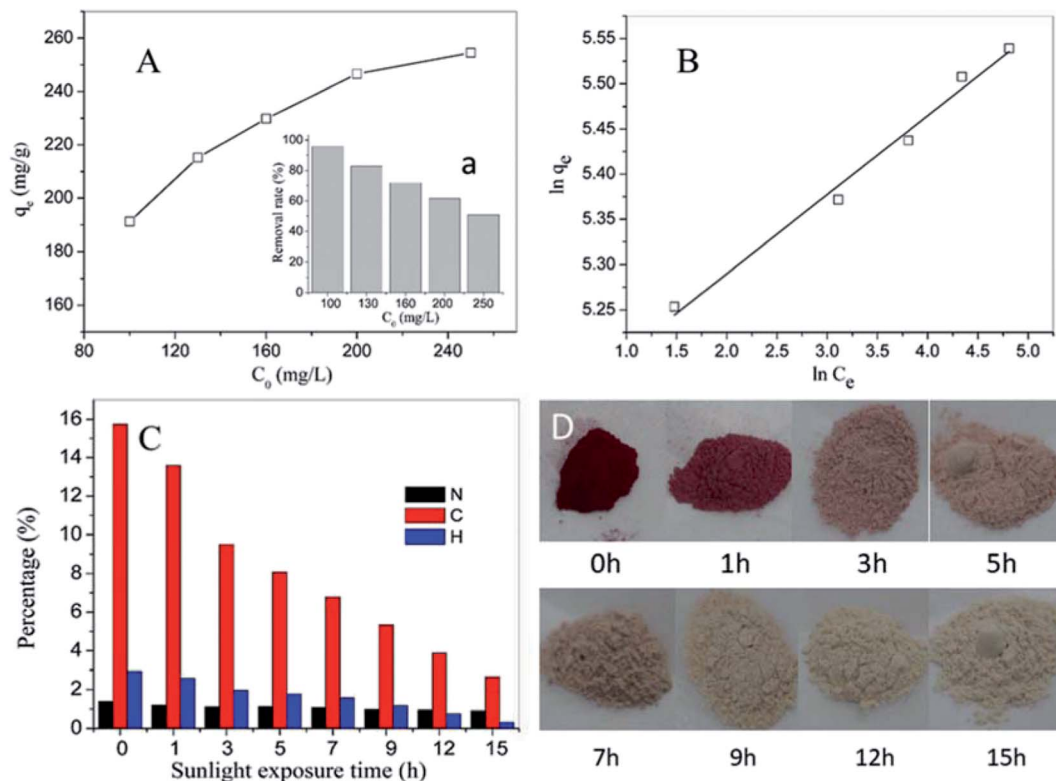
Fig. 9 Saturated adsorption of the photocatalyst for X3B (A), the corresponding fitted kinetic curves (B), the C, N, H mass percentage and photo of the slurry from absorption of X3B (C and D) under different sunlight exposure time.
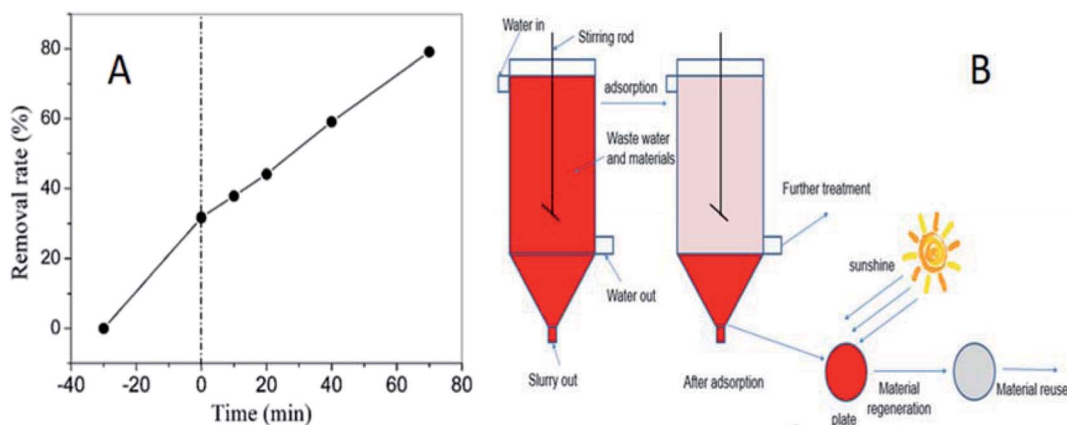

Fig. 10 The photocatalytic performance for the regenerated material (A), the potential way of application for SN–SiO₂–BiOBr (B).

taken in solid phase. For C, N and H elements content, they decrease with the sunlight exposure time. The final content of C, N and H is 2.649, 0.909 and 0.313%, respectively. For C element content, after 15 h exposure it is decreased by 83.2%, which is 34% for N elements, 89.4% for H elements. During this process X3B and SN is almost degrade to CO_2, NO_2 and H_2O. Fig. 9D shows the color change with the exposure time for X3B slurry. The color was faded from red to light gray. In this process, the samples were regenerated. 5 mg slurry irradiated for 15 h was used to degrade 20 mg L^{-1} X3B without further treatment. The results are shown in Fig. 10A. After 70 min

irradiation, the removal rate is around 80%. On the basis of above results, the potential way of application is shown in Fig. 10B.

4. Conclusion

The xSiO₂–BiOBr (x = 0–5) nanoparticles are prepared via a facile one-step co-precipitation process. 4SiO₂–BiOBr shows a better photocatalytic efficiency than other composites. The addition of sodium metasilicate not only provide the silicon source but also adjust the pH value, which both are beneficial to

photocatalytic performance of the resulted composites. Due to the mutual contaction of the interfaces of SiO_2 and BiOBr, the visible light adsorption ability is increased. Under the help of the active species analysis in the photocatalytic degradation of X3B, a detailed degradation mechanism of X3B degradation by $4SiO_2$–BiOBr composite was proposed. The $O_2^{\cdot-}$ and h^+ were proved to be the main active species in the photocatalytic reaction with X3B. For the intended purposes, the SN–SiO_2–BiOBr was synthesized by using an identical process, but with the addition of an organic component of SN. The adsorption performance of the resulted hybrid was much higher than that of $4SiO_2$–BiOBr, which was attributed to the electric charge effect with SN. And it was innovatively used for the photocatalytic degradation in concentrated slurry under sunlight irradiation for the first time. The pollutants could be totally degraded to H_2O and CO_2. The recycling experiment demonstrated that the hybrid also can be reused. As a result, by using the newly-fabricated hybrid, the load of sewage could be dramatically reduced, which greatly facilitates the treatment of wastewater contaminated by organic pollutants.

Conflicts of interest

There are no conflicts to declare.

Acknowledgements

References

1 W. Jiang, Y. Liu, J. Wang, M. Zhang, W. Luo and Y. Zhu, *Adv. Mater. Interfaces*, 2016, **3**, 1500502.

2 H. Wang, X. Yuan, Y. Wu, G. Zeng, H. Dong, X. Chen, L. Leng, Z. Wu and L. Peng, *Appl. Catal., B*, 2016, **186**, 19–29.

3 N. D. McNamara and J. C. Hicks, *ACS Appl. Mater. Interfaces*, 2015, **7**, 5338–5346.

4 Y. Liang, S. Lin, L. Liu, J. Hu and W. Cui, *Appl. Catal., B*, 2015, **164**, 192–203.

5 F. Dong, Q. Li, Y. Zhou, Y. Sun, H. Zhang and Z. Wu, *Dalton Trans.*, 2014, **43**, 9468–9480.

6 Y. Zhu, Y. Wang, Q. Ling and Y. Zhu, *Appl. Catal., B*, 2017, **200**, 222–229.

7 Y. Mi, L. Wen, Z. Wang, D. Cao, R. Xu, Y. Fang, Y. Zhou and Y. Lei, *Nano Energy*, 2016, **30**, 109–117.

8 S. Gao, C. Guo, J. Lv, Q. Wang, Y. Zhang, S. Hou, J. Gao and J. Xu, *Chem. Eng. J.*, 2017, **307**, 1055–1065.

9 S. Ning, H. Lin, Y. Tong, X. Zhang, Q. Lin, Y. Zhang, J. Long and X. Wang, *Appl. Catal., B*, 2017, **204**, 1–10.

10 L. Ye, Y. Su, X. Jin, H. Xie and C. Zhang, *Environ. Sci.: Nano*, 2014, **1**, 90.

11 J. Ke, X. G. Duan, S. Luo, H. Y. Zhang, H. Q. Sun, J. Liu, M. Tade and S. B. Wang, *Chem. Eng. J.*, 2017, **313**, 1447–1453.

12 Z. Zhang, Y. Zhou, S. Yu, M. Chen and F. Wang, *Mater. Lett.*, 2015, **150**, 97–100.

13 H. Li and L. Z. Zhang, *Nanoscale*, 2014, **6**, 7805–7810.

14 Y. Wu, Q. Han, L. Wang, X. Jiang, X. Wang and J. Zhu, *J. Environ. Chem. Eng.*, 2017, **5**, 987–994.

15 H. Li, N. Li, D. Chen, Q. Xu and J. Lu, *Appl. Surf. Sci.*, 2017, **403**, 80–88.

16 Z. Haider, J. Y. Zheng and Y. S. Kang, *Phys. Chem. Chem. Phys.*, 2016, 19595–19604.

17 Y. Huo, J. Zhang, M. Miao and Y. Jin, *Appl. Catal., B*, 2012, **111–112**, 334–341.

18 H. Gnayem and Y. Sasson, *ACS Catal.*, 2013, **3**, 186–191.

19 Z. Jiang, F. Yang, G. D. Yang, L. A. Kong, M. O. Jones, T. C. Xiao and P. P. Edwards, *J. Photochem. Photobiol., A*, 2010, **212**, 8–13.

20 J. Di, J. Xia, M. Ji, B. Wang, S. Yin, Q. Zhang, Z. Chen and H. Li, *Appl. Catal., B*, 2016, **183**, 254–262.

21 J. Di, J. X. Xia, M. X. Ji, B. Wang, X. W. Li, Q. Zhang, Z. G. Chen and H. M. Li, *ACS Sustainable Chem. Eng.*, 2016, **4**, 136–146.

22 H. Li, J. Shang, Z. H. Ai and L. Z. Zhang, *J. Am. Chem. Soc.*, 2015, **137**, 6393–6399.

23 J. X. Xia, J. Di, H. T. Li, H. Xu, H. M. Li and S. J. Guo, *Appl. Catal., B*, 2016, **181**, 260–269.

24 D. Wu, L. Q. Ye, H. Y. Yip and P. K. Wong, *Catal. Sci. Technol.*, 2017, **7**, 265–271.

25 X. Geng, W. Li, F. Xiao, D. Wang and L. Yang, *Catal. Sci. Technol.*, 2017, **7**, 658–667.

26 J. Di, J. Xia, M. Ji, B. Wang, X. Li, Q. Zhang, Z. Chen and H. Li, *ACS Sustainable Chem. Eng.*, 2016, **4**, 136–146.

27 W. Li, X. Jia, P. Li, B. Zhang, H. Zhang, W. Geng and Q. Zhang, *ACS Sustainable Chem. Eng.*, 2015, **3**, 1101–1110.

28 L. Zhang, W. Wang, S. Sun, Y. Sun, E. Gao and Z. Zhang, *Appl. Catal., B*, 2014, **148–149**, 164–169.

29 Y. R. Yao, W. Z. Huang, H. Zhou, H. Y. Yin, Y. F. Zheng and X. C. Song, *Mater. Chem. Phys.*, 2014, **148**, 896–902.

30 Y. T. Wei Li, P. Li, B. Zhang, H. Zhang, W. Geng and Q. Zhang, *RSC Adv.*, 2015, 48050–48059.

31 W. J. Kim, D. Pradhan, B. K. Min and Y. Sohn, *Appl. Catal., B*, 2014, **147**, 711–725.

32 X. Q. Yan, X. H. Zhu, R. H. Li and W. X. Chen, *J. Hazard. Mater.*, 2016, **303**, 1–9.

33 B. Priya, P. Raizada, N. Singh, P. Thakur and P. Singh, *J. Colloid Interface Sci.*, 2016, **479**, 271–283.

34 Y. C. Yu, Z. J. Hu, Y. L. Zhang and H. W. Gao, *RSC Adv.*, 2016, **6**, 18577–18582.

35 Y.-P. Wei and H.-W. Gao, *J. Mater. Chem.*, 2012, **22**, 5715.

36 H. W. Gao, G. Xu and Y. Wang, *RSC Adv.*, 2014, **4**, 23690–23693.